Gating-induced Mott transition in NiS_2

Ezra Day-Roberts,[1,2] Rafael M. Fernandes,[1] and Turan Birol[2]
[1]*School of Physics and Astronomy, University of Minnesota, Minneapolis, Minnesota 55455, USA*
[2]*Department of Chemical Engineering and Materials Science, University of Minnesota, Minnesota 55455, USA*

(Received 24 March 2022; revised 11 February 2023; accepted 13 February 2023; published 28 February 2023)

NiS_2 has been widely regarded as a model system to study the bandwidth-controlled Mott transition, as enabled by isovalent Se chemical substitution on the S sites. Motivated by advances in electrostatic gating, we theoretically investigate the filling-controlled Mott transition induced by gating, which has the advantage of avoiding disorder introduced by dopants and stoichiometric changes. We use combined density-functional theory (DFT) and dynamical mean-field theory (DMFT) to study such a filling-controlled transition and compare it with the case of bandwidth control. We draw a temperature-filling phase diagram and find that the Mott-insulator to metal transition occurs with modest added electron concentrations, well within the capabilities of existing electrostatic gating experiments. We find that there is significant incoherent weight at the Fermi level in the metallic phase when the transition is induced by gating. In contrast, the spectral weight remains rather coherent in the case of the bandwidth-controlled transition.

DOI: 10.1103/PhysRevB.107.085150

I. INTRODUCTION

While a simple quantum-mechanical description of noninteracting electrons is sufficient to explain the insulating phase of materials with fully occupied atomic orbitals [1], it was realized early on that interactions between electrons need to be taken into account to explain the insulating nature of compounds with partially filled transition-metal *d* orbitals such as NiO [2,3]. In these so-called Mott insulators, the onsite-screened Coulomb repulsion out-competes the kinetic energy gained by delocalized electrons, resulting in an insulating phase with localized electrons. While most Mott insulators undergo a temperature-driven metal-to-insulator transition (MIT) before they melt [4–8], another interesting scenario is that in which the MIT can be triggered at fixed temperature by tuning the material properties [9]. These transitions are the subject of ongoing interest due to both a plethora of interesting emergent phenomena associated with the MIT, including possible quantum critical behavior [10–13].

At a fixed temperature, metal-insulator transitions can be induced by changes in the electron-electron interaction strength, the bandwidth, or the band filling, i.e., the number of valence electrons per atom [10]. While theoretical models enable studying the effects of all of these parameters separately, experiments typically focus on the latter two [9]. Bandwidth is typically tuned by either hydrostatic or chemical pressure, which refers to the isovalent substitution of atoms that preferably do not have any electronic states near the Fermi level. A typical example of chemical pressure is substitution of the A-site cations in perovskite oxides, which are typically either alkaline-earth or rare-earth elements, with other isovalent alkaline-earth or rare-earth atoms (for example, see Ref. [14]). These substitutions change the unit-cell volume and internal structural parameters, but do not affect the number of electrons in the bands near the Fermi level. Anion substitution, such as sulfurization of oxides, can also be used to induce chemical pressure and change the crystal structural parameters (for example, see Refs. [15,16]). But a more important effect of anion substitution in transition-metal oxides is the change in the hopping amplitude t between transition-metal orbitals, which modifies the bandwidth near the Fermi level.

Aliovalent doping changes the number of electrons, and is the most commonly used means to change the electron filling. For example, substituting the rare-earth atoms in rare-earth titanate perovskites with alkaline-earth elements adds a hole, which can move the system away from integer-filling, and hence lead to a metallic phase [17]. However, this approach has two shortcomings when used to study filling-induced Mott transitions: (1) Since no two ions have exactly the same radius, chemical doping necessarily has a steric effect that changes the crystal structure. Hence, it is not solely a change of electron filling. (2) Partial substitution of an element with another rarely results in an ordered crystal structure. Instead, a random distribution of dopant atoms is more common. This results in local disorder in both the crystal structure and the electrostatic potential the electrons experience [18,19].

Recently, electrolyte gating approaches that rely on ionic liquids or gels have emerged as an alternate means to modify the carrier concentration and induce phase transitions in solids [20–22]. By using an electric double-layer transistor device, it is possible to obtain electrostatic as well as electrochemical effects and induce charge densities that are well beyond what can be achieved by using solid dielectrics [23,24]. This approach was shown to be successful in, for example, modifying the superconducting properties of $SrTiO_3$ [25], $KTaO_3$ [26], and various cuprates [27–29]; inducing metal-insulator transitions in WO_3 [30] and nickelate perovskites [31,32]; or inducing ferromagnetism in

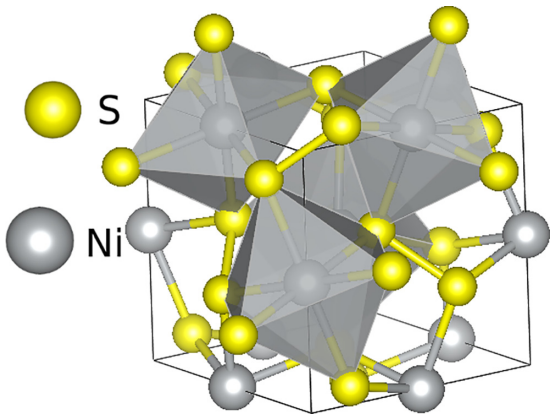

FIG. 1. The pyrite crystal structure. Gray and yellow atoms represent the transition metal (in this case Ni) and sulfur ions, respectively. The Ni–S and S–S bonds have lengths of 2.39 Å and 2.07 Å, respectively.

diamagnetic FeS_2 [33,34]. In addition to changing the band filling without necessarily introducing chemical or structural inhomogeneities, gating approaches also help bridge the miscibility gaps in compounds where suitable dopants are not easily identified.

NiS_2 is a well studied Mott insulator, which provides a fertile playground to examine the metal-insulator transition. It has the pyrite structure named after FeS_2 (Fig. 1) [35,36]. With its cubic symmetry and simple stoichiometry, as well as the availability of large single crystals and solid solutions [37,38], it was considered as a model system to study the Mott transition as early as the 1970s [39,40]. Sulfur is a chalcogen one row below oxygen in the periodic table and similar to oxygen the most common anion of sulfur is S^{2-} sulfide; however, in the pyrite structure, sulfur ions form S–S dimers, which have a total charge of -2 per dimer. The S–S distance is 2.07 Å, closer to elemental S_2 with $d_{S-S} = 1.887$ Å [41] and far from the S–S distances in compounds without S–S bonding, such as the perovskite $BaZrS_3$ with $d_{SS} = 3.58$ Å. One unusual feature of this structure is the existence of covalently bonded chalcogen dimers, which are marked with bonds in Fig. 1. In contrast with most oxide structures where the chalcogens each have a charge of -2, here the sulfur dimer collectively has a charge of -2, giving each sulfur an individual ionization of -1. In addition to the filling-controlled transition achieved by doping the transition-metal site, a bandwidth-controlled transition can be achieved by partially substituting S by Se [42,43]. Note that $NiSe_2$ is a Pauli paramagnetic metal, whereas NiS_2 is a Curie-Weiss paramagnet that orders antiferromagnetically below 38 K [44–46]. There is now a large body of work focused on $NiS_{2-x}Se_x$ that includes both experimental and theoretical studies [47–54]. The body of first-principles work on $NiS_{2-x}Se_x$ includes a number of dynamical mean-field theory (DMFT) studies, starting from as early as 1998 [55], and, most recently, the discussion of Hund metal behavior near the transition [56].

In this paper, we study the metal-insulator transition in electron-doped NiS_2 using first principles density-functional theory plus embedded dynamical mean-field theory (DFT + eDMFT) [57–59]. In particular, we consider the electrostatically or electrolyte gated system without chemical doping or electrochemical changes, where the electron concentration increases without any change in the stoichiometry of the system. We thus focus on the carrier filling induced Mott transition, which we compare with the bandwidth-induced transition in the Se substituted system. The behavior of this system under electrostatic gating is of interest because of the successful application of the gating approach to the closely related compound FeS_2 [34], as well as the recent experiments on NiS_2 that demonstrate a metal-insulator transition under gating [60]. However, the role of electrostatic-only effects in these experiments is unclear [24], and a theoretical answer to the question of whether such a transition is feasible in the experimentally achievable electron concentrations is missing so far.

Our results show that a very small electron concentration, well within the reach of electrolyte gating, is sufficient to suppress the Mott insulating phase. By computing the spectral density and the quasiparticle spectral weight, we also find that the filling-induced transition is different from the one induced by changing the bandwidth in key points. Specifically, the former leads to a highly incoherent metallic phase and to features in the density of states (DOS) reminiscent of the Mott gap. This is in contrast with the bandwidth induced transition, where the gap completely collapses in the metallic phase.

The paper is organized as follows: Section II introduces the DFT + DMFT methodology. The crystal and electronic structures of undoped NiS_2 are discussed in Sec. III, whereas Sec. IV presents the DFT + eDMFT results for the DOS and the quasiparticle spectral weight. Section V is devoted to the conclusions.

II. METHODS

Density-functional theory + embedded dynamical mean-field theory (DFT + eDMFT) calculations were performed using the Rutgers eDMFT code [58,61]. The density-functional theory calculations using the local density approximation were performed using the linearized augmented plane-wave method as implemented in WIEN2K [62]. A $10 \times 10 \times 10$ k-point grid was used for the 12 atom primitive unit cell of NiS_2. The DMFT problem was solved via the continuous time quantum Monte Carlo solver included in the eDMFT code. The self-energy was directly sampled and its high-frequency tail was smoothed for stability as described in Ref. [63]. The Ni $3d$ orbitals were treated in DMFT with localized states constructed as described in Ref. [58]. In this unit cell, the local axes of each Ni ion are oriented differently, but all atoms are symmetry equivalent, i.e., there is only one Wyckoff position for Ni, and another one for S. As a result, a single Ni ion was considered as the impurity in the DFT + eDMFT calculations. The Green's function and self-energies for the orbitals on the other Ni ions were generated by applying space group operations that interchange the Ni ions. All five $3d$ orbitals of the Ni ions were included in the impurity problem, even though the t_{2g} manifold is completely filled. The on-site Hubbard U and Hund's J parameters were set to 10.7 and 0.7 eV, which were shown in multiple references (for example, Refs. [64,65]) to be suitable for $3d$ transition metals for the implementation that we use. This number is larger than the typically used values in

DFT + U, as well as other DFT + DMFT implementations, due to the facts that DMFT explicitly takes into account certain screening processes and that our DMFT implementation does not use less localized Wannier orbitals as the correlated orbitals. Hybridization with all the states in a wide energy window that spans ∓ 10 eV around the Fermi level was taken into account, and all transition-metal orbitals were explicitly included in the impurity calculation. This latter point also has an effect on the value of U, since taking into account the Feynman diagrams involving the occupied d orbitals explicitly in the impurity calculation requires not reducing the value of U due to screening by those orbitals. The "exact" double-counting approach was used in all calculations [66].

Unless otherwise stated, the experimental crystal structure of NiS_2 from Ref. [67] was used in all calculations. While the added electrons can change bonding and effective ionic radii, and hence change the crystal structure [33,68], this effect is not expected to be significant at the small concentrations considered at this work and hence is ignored. The lattice constant for $Ni(S_{0.75}Se_{0.25})_2$ was linearly interpolated between endpoints NiS_2 and $NiSe_2$ and the atomic positions were determined by relaxation in WIEN2K (at the DFT level).

The fully self-consistent DFT + DMFT implementation we use does not allow changing the number of electrons independently in the DFT and the DMFT loops. We added electrons to the system by changing the total number of electrons in the DFT calculation along with a homogeneous background charge to keep the system charge neutral [69]. The added electrons lead to a change in the impurity occupation in the DMFT calculation.

III. CRYSTAL AND ELECTRONIC STRUCTURES OF NiS_2: DFT RESULTS

The pyrite crystal structure shown in Fig. 1 is commonly found in the 3d transition-metal disulfides, other examples being FeS_2, CuS_2, and CoS_2 [70]. Despite its primitive cell that contains four formula units, the pyrite structure is highly symmetric and has the simple cubic space group $Pa\bar{3}$ (#205) [67]. The transition-metal ions occupy the corners and the face-centers of the cubic unit cell, or equivalently the edge-centers if a shifted origin is chosen. Sulfur ions form octahedra around each transition metal. The orientations of these octahedra are not the same with respect to each other, which leads to the simple cubic symmetry rather than the face-centered cubic one. The structure is centrosymmetric with various screw axes and glide planes, and there are threefold roto-inversion axes along all body diagonals. Due to these symmetry operations, every transition-metal ion is chemically equivalent, with different local axes, i.e., they occupy a single Wyckoff position 4a. Similarly, all sulfur ions are chemically equivalent.

The previously mentioned covalent bonding in the sulfur dimers gives rise to unoccupied antibonding sulfur bands near the Fermi level [44,71]. The octahedral coordination environment of the transition-metal cations gives rise to a significant t_{2g}-e_g splitting of their d orbitals. This splitting is responsible, for example, for the band-insulating behavior of FeS_2, as Fe has completely filled t_{2g} and completely empty e_g orbitals [72]. The Ni^{2+} ions in NiS_2 have eight electrons in

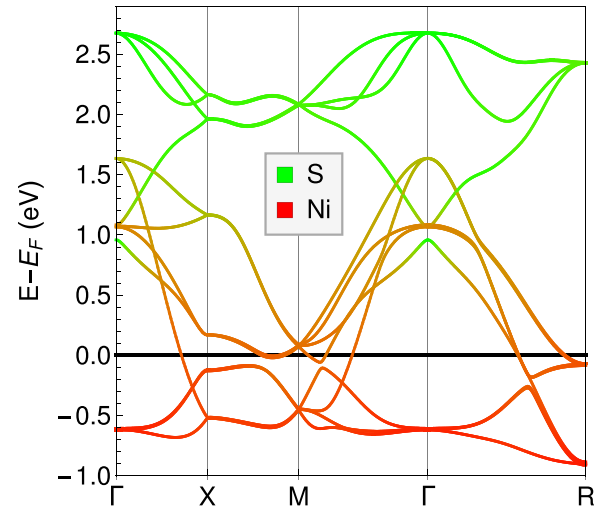

FIG. 2. Band structure of nonmagnetic NiS_2 from density-functional theory. The wave function of each band at each wave vector is projected onto Ni and S states to obtain the atomic characteristics of the bands. The higher lying bands arise from the sulfur dimer antibonding orbitals and hence are almost purely of S character. However, these bands overlap with the bands with Ni-e_g character, mixing with them at lower energies.

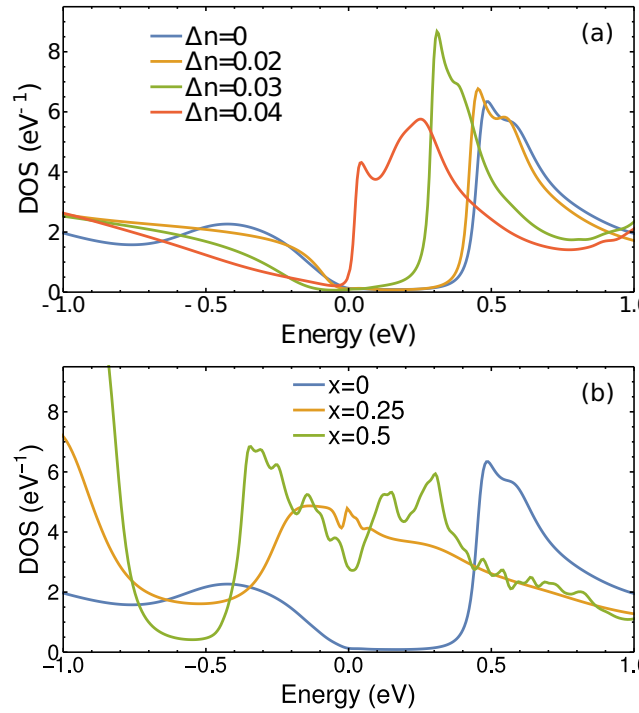

FIG. 3. Evolution of the DOS of NiS_2 under (a) electrostatic gating and (b) Se substitution. Panel (a), obtained at a constant temperature of $T = 223$ K, shows that the Mott gap slowly closes upon increasing the number of electrons per Ni ion, Δn. At $\Delta n = 0.04$ the Fermi level has moved into the upper Hubbard band, but there is still a clear suppression of the DOS immediately below it. Panel (b) refers to the isovalent substituted $Ni(S_{1-x}Se_x)_2$ at the same temperature. Note that the Mott gap completely collapses for $x = 0.25$.

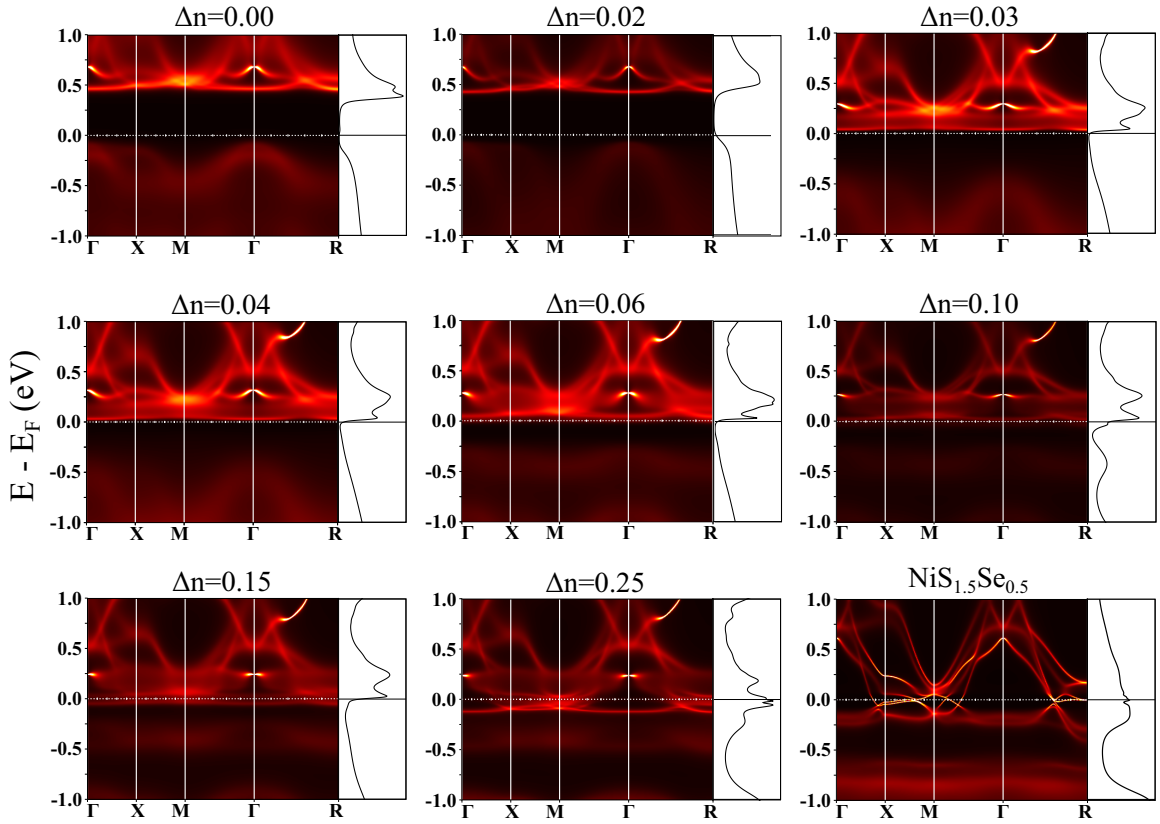

FIG. 4. Evolution of the spectral function $A(k, \omega)$ of NiS_2 as a function of increasing electron concentration Δn, and also for the case of 25% Se substitution. All plots are from calculations performed at $T = 223$ K. The DOS curves are shown in the right side of each panel. According to the self-energies shown in Fig. 5, the systems shown in the first three plots ($\Delta n \leqslant 0.03$) exhibit insulating behavior.

their partially filled d shell. This results in completely filled t_{2g} orbitals and half filled e_g orbitals [71].

The non-spin-polarized DFT band-structure of NiS_2 is shown in Fig. 2. Without magnetic moments or a $+U$ correction, DFT predicts this material to be metallic. The Fermi level crosses the eight-band Ni-e_g manifold, which is separated in energy from the Ni-t_{2g} and occupied sulfur p bands. The sulfur antibonding orbitals give rise to four unfilled bands, which are located in the range 1.0–2.5 eV above the Fermi level. Because these bands overlap and mix with the Ni-e_g bands, even the lower-energy Ni-e_g bands have significant sulfur character, indicating the relatively covalent nature of this material.

At $T_N \approx 38$ K, NiS_2 undergoes a phase transition to a noncollinear antiferromagnetic insulating phase with $S = 1$ moments formed by the parallel alignment of the spins of the two electrons on the Ni e_g orbitals [46,73,74]. While it remains an insulator in the paramagnetic phase, a Mott-insulator to metal transition can be induced by doping [40], pressure [75,76], or isovalent substitution of S with Se [39,42,54]. The metal-insulator transition induced by Se substitution has been studied in great detail both theoretically and experimentally [9,47–55], and is considered to be a relatively clean example of bandwidth-controlled Mott transition. This is because Se is a neighbor of S in the periodic table, such that its substitution is not expected to introduce strong disorder on the transition-metal site.

IV. CORRELATED ELECTRONIC SPECTRUM: DFT + eDMFT RESULTS

In Fig. 3(a), we show the density of states (DOS) of NiS_2 obtained from DFT + eDMFT calculations as a function of electron doping induced by electrostatic gating. Doping is simulated by adding electrons at the DFT level and allowing this to propagate to the DMFT portion via full charge self-consistency. The number of electrons in the unit cell is modified in WIEN2K along with the addition of a homogeneous background charge to maintain charge neutrality. At the temperature we consider ($T = 223$ K), undoped NiS_2 is a Mott insulator with a well-defined gap and minimal incoherent weight at this gap. Increasing the number of electrons as much as $\Delta n = 0.03$ e^- per Ni ion shifts the Fermi level up while at the same time increasing the DOS in the gap slightly, even though a gap remains visible. The Fermi level E_F crosses the bottom of the conduction band and the DOS at E_F becomes significant when $\Delta n = 0.04$, suggesting the onset of metallic behavior. Nevertheless, a dip in the DOS below the Fermi level persists, resembling a remnant gap. These features are resilient to details of analytic continuation, see the Supplemental Material, Fig. S.1 [77]. This behavior is in contrast to the bandwidth-controlled MIT in $Ni(S_{1-x}Se_x)_2$. As shown in Fig. 3(b), even when 25% of S atoms are substituted with isovalent Se, the Mott gap completely collapses, and any

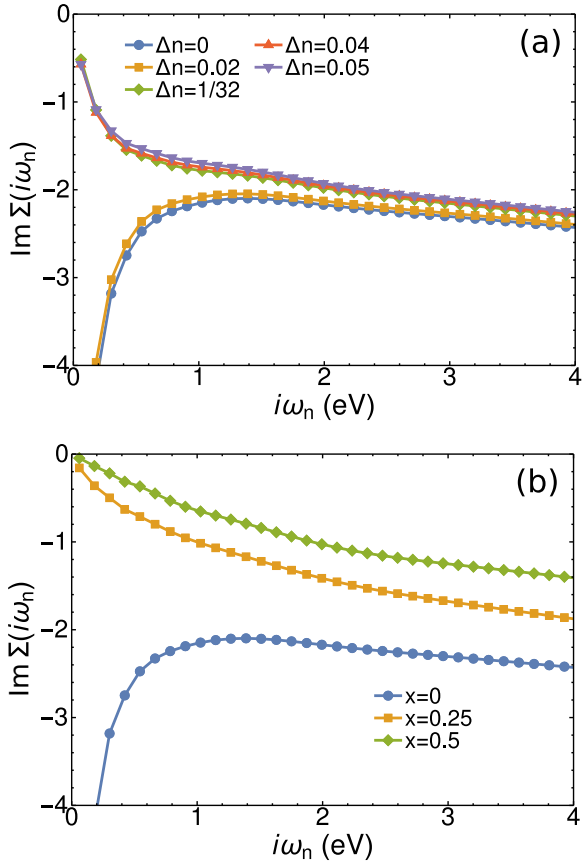

FIG. 5. (a) The imaginary part of the self-energy on the Matsubara axis, $\mathrm{Im}\Sigma(i\omega)$, shows a clear MIT upon increasing electron concentration around the value of $\Delta n = 1/32$ added electrons per Ni ion. Even in the metallic state, the compound shows strong electron-electron scattering and correlations as evinced by the nonzero intercept of $\mathrm{Im}\Sigma(i\omega)$ and its large slope approaching zero Matsubara frequency. (b) The imaginary part of the self-energy of Se-substituted $Ni(S_{1-x}Se_x)_2$ also shows a clear MIT when $x = 25\%$. In the metallic state, although the slope of $\mathrm{Im}\Sigma(i\omega)$ indicates the presence of bandwidth renormalization, the compound is a good metal since $\mathrm{Im}\Sigma(i\omega)$ has essentially a zero intercept with the $\omega_n = 0$ axis.

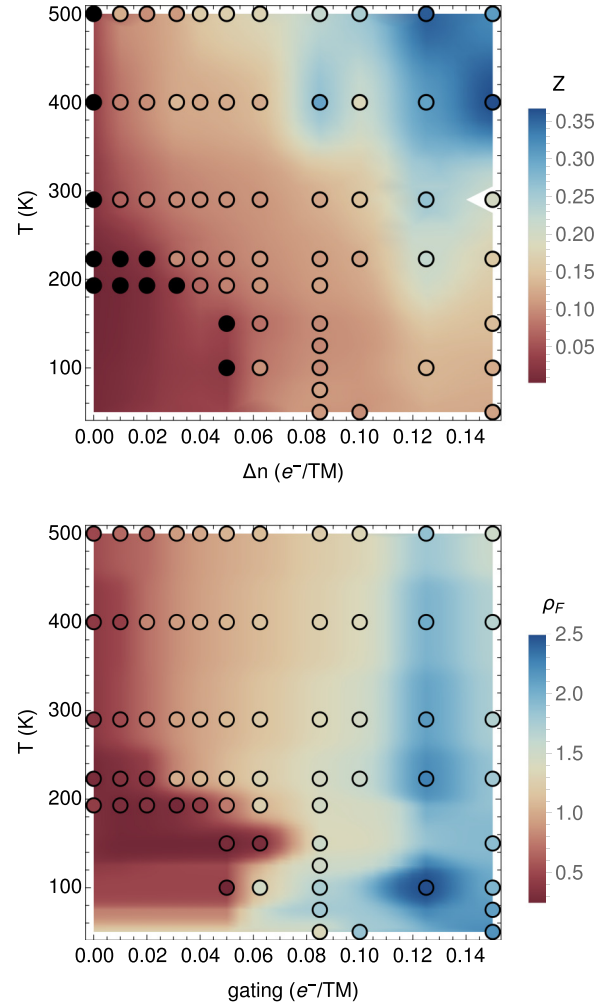

FIG. 6. Gating-temperature (in terms of the number of added electrons per Ni atom) phase diagrams showing both the quasiparticle spectral weight Z (top), and the proxy to the DOS at the Fermi level ρ_F (bottom), as defined in the main text. Circles indicate the values where the DFT + eDMFT calculations were performed and insulating points in the upper figure are marked with solid black dots. The phase diagram was then obtained using a linear interpolation scheme.

feature resembling a gap is completely absent. The latter is consistent with what was previously reported in Ref. [53].

To gain further insight into the differences between filling-controlled (gating) and bandwidth-controlled (Se substitution) Mott transitions, we show in Fig. 4 the spectral functions $A(k, \omega)$ in both situations. In the case of doping, the Hubbard band at the bottom of the conduction manifold remains nearly unchanged with increasing Δn, despite the fact that the gap in the DOS is slowly filled with incoherent states. Even for $\Delta n > 0.06$, where the DOS is nonzero at the Fermi level, and the Fermi level starts crossing the upper Hubbard band of the undoped compound, there are no clearly defined dispersive bands. This is consistent with a correlated metallic state where most of the spectral weight is incoherent, including near the Fermi level. In contrast, the 25% Se-substituted system has sharp bands crossing the Fermi level, indicative of a coherent metallic regime.

To more quantitatively assess these behaviors, we show the imaginary part of the self-energy on the Matsubara axis, $\mathrm{Im}\Sigma(i\omega)$, because it can be used to gauge the strength of electronic correlations in the metallic state. Specifically, following the method of Ref. [78], the slope of $\mathrm{Im}\Sigma(i\omega)$ as $\omega \to 0$ is related to the quasiparticle weight Z via

$$Z^{-1} = 1 - \left.\frac{\partial \mathrm{Im}\Sigma(i\omega)}{\partial \omega}\right|_{\omega\to 0}. \quad (1)$$

We fit a fourth-degree polynomial to the lowest five Matsubara frequencies and extract the linear component. Thus, a large negative slope indicates strong correlations (i.e., a small Z), whereas a divergent positive slope signals a Mott insulating phase (i.e., $Z = 0$). The advantage of using this expression for calculating Z, rather than a similar expression on the real frequency axis, is that it does not require the use of numerical analytical continuation methods such as the maximum entropy method, which are bound to introduce errors. The results from this do not depend sensitively on the degree of polynomial

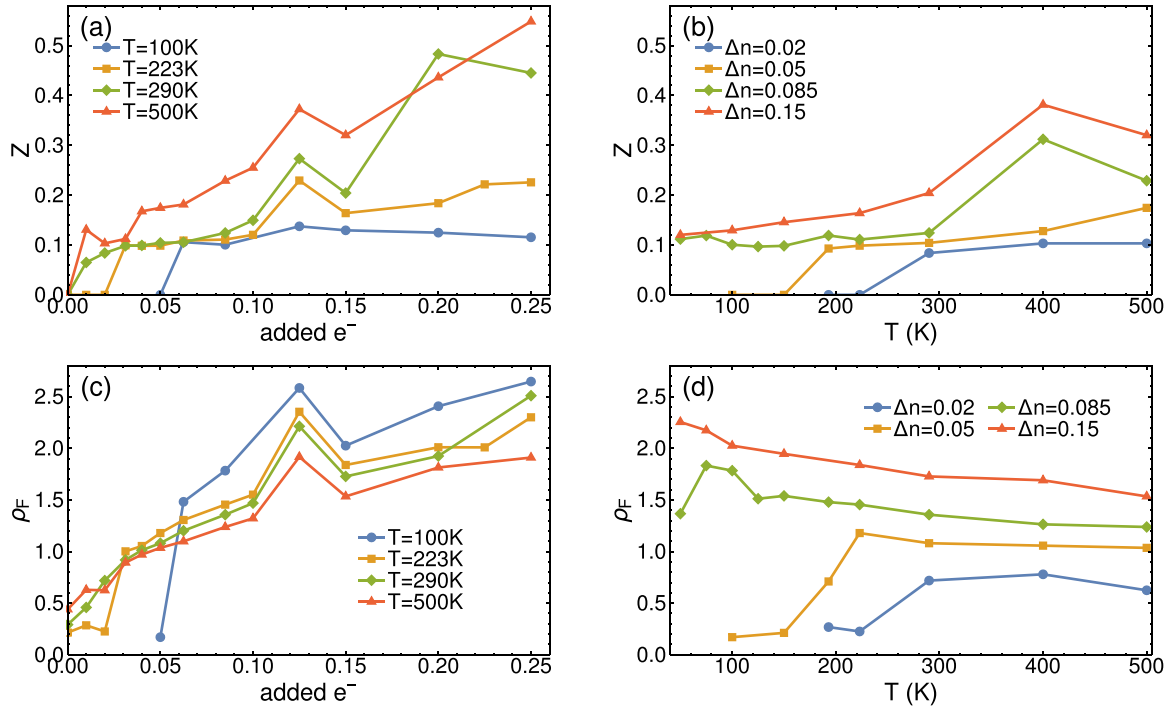

FIG. 7. The quasiparticle spectral weight Z (top) and the proxy for the DOS at the Fermi level ρ_F (bottom) along cuts of constant temperature T (left) and constant doping Δn (right) in the Δn-temperature phase diagram of Fig. 6.

or number of points fit, see Fig. S.2 of the Supplemental Material [77].

The self-energy $\Sigma(i\omega)$ of the e_g orbitals is shown in Fig. 5(a) for different values of electron doping Δn. For smaller Δn values, the self-energy is divergent, signaling a Mott-insulating phase. For larger doping values, however, $\Sigma(i\omega)$ displays a sizable but doping-independent slope, signaling a correlated metallic phase. The imaginary part of the self-energy in the metallic phase has a nonzero intercept for all metallic doping levels, consistent with large electron-electron scattering and a large degree of remaining incoherent weight. The finite-temperature Mott transition is described by a first-order transition line terminating at a critical endpoint [6,79]. Although we are not able to determine this endpoint from our calculations, it is unlikely to extend to high temperatures. Thus, since we see a sharp change in the asymptotic behavior of the self-energy as a function of Δn, we use this criterion to delineate the metallic and insulating phases in the doping-temperature phase diagram. In comparison to the electron-doping case, the self-energy in the Se substitution case displays a very small intercept [Fig. 5(b)], consistent with there being less scattering and less incoherent weight at the Fermi level. Indeed, while the bandwidth is renormalized significantly [$Z = 0.22$ for $Ni(S_{0.75}Se_{0.25})_2$], the bands in Fig. 4 appear "sharp" and hence coherent.

In Fig. 6 we present the gating (in terms of the number of added electrons per Ni atom, Δn) *versus* temperature phase diagram of NiS_2. The quasiparticle residue Z is shown together with the imaginary axis Greens's function evaluated at the lowest Matsubara frequency, $\rho_F = -\mathrm{Im}\mathrm{Tr}G(i\omega_0)$, which is a proxy for the density of states at the Fermi level. These two quantities show slightly different trends, but are in good agreement within the error bars. Indeed, the points displaying Mott insulating behavior ($Z = 0$) coincide with those with almost zero DOS at the Fermi level, $\rho_F \approx 0$. Undoped NiS_2 is insulating at all temperatures up to 500 K in our calculations, but the temperature range of the insulating region on the phase diagram narrows with the introduction of electrons via gating. The system develops a nonzero Z (and hence becomes metallic) with the addition of even 0.01 electrons per formula unit above a temperature of about ≈220 K. Below this temperature, there is a wider insulating region, extending to $\Delta n \approx 0.05$. Above concentrations of $\Delta n \approx 0.06$, there is a sizable DOS at the Fermi level at all temperatures, whereas Z increases significantly with increasing temperature. Throughout the region spanned by the temperature-doping values we considered, NiS_2 remains significantly correlated, with Z remaining below 0.35.

Figure 7 shows selected line cuts through the phase diagrams in Fig. 6. While the fixed-temperature Z curves depend sensitively on the doping level [Fig. 7(a)], the DOS (ρ_F) curves are relatively insensitive to temperature, particularly at higher temperatures in the metallic phase [Fig. 7(c)]. However, both the temperature at which Z drops to zero [Fig. 7(b)] and the temperature at which there is a sudden drop in ρ_F [Fig. 7(d)] clearly depend on the value of Δn, with no such drops being observed in either quantity above $\Delta n \approx 0.06$.

V. CONCLUSIONS

Recent developments in electrostatic gating opened new avenues of research where the carrier concentrations in materials can be tuned continuously without necessarily introducing disorder or stoichiometric effects. Here, we used first principles DFT + eDMFT to study a filling induced metal-insulator transition in the Mott insulating transition-metal

sulfide NiS_2. Although DFT + eDMFT provides a more realistic setting than DMFT alone, there are still phenomena, such as polarons [80] and Wigner localization [81], that we are not able to capture. If these effect suppress Mottness, they could possibly lead to an even lower carrier concentration needed to induce the metallic state. Our calculations show that the spectral properties behave very differently when a Mott transition is induced by changing carrier concentration (filling control) rather than by isovalent chemical substitution (bandwidth control). Increasing the carrier concentration leaves the system with significant incoherent spectral weight, while bandwidth manipulation via Se substitution creates coherent bands and minimal incoherent weight at the Fermi level. Our results further show that metal-insulator transitions at a wide range of temperatures can be induced in NiS_2 under modest doped electron concentrations. A concentration of $\Delta n = 0.06$ additional electrons per Ni atom corresponds to a surface electron density of $\approx 8 \times 10^{13}\ e^-/\mathrm{cm}^2$, assuming the gating penetrates exactly one unit cell, well within the capabilities of electrostatic gating [22]. Our results show that electrostatic gating can provide a complementary means to study the Mott transition via introducing carriers with minimum disorder.

ACKNOWLEDGMENTS

We thank C. Leighton and J. Walter for fruitful discussions. This work was supported primarily by the National Science Foundation through the University of Minnesota MRSEC under Award No. DMR-2011401.

[1] J. C. Slater, The electronic structure of metals, Rev. Mod. Phys. **6**, 209 (1934).
[2] N. F. Mott and R. Peierls, Discussion of the paper by de Boer and Verwey, Proc. Phys. Soc. **49**, 72 (1937).
[3] N. W. Ashcroft and N. D. Mermin, *Solid State Physics* (Saunders College, Philadelphia, 1976).
[4] P. Limelette, A. Georges, D. Jérome, P. Wzietek, P. Metcalf, and J. Honig, Universality and critical behavior at the Mott transition, Science **302**, 89 (2003).
[5] K. Kanoda and R. Kato, Mott physics in organic conductors with triangular lattices, Annu. Rev. Condens. Matter Phys. **2**, 167 (2011).
[6] G. Kotliar, E. Lange, and M. J. Rozenberg, Landau Theory of the Finite Temperature Mott Transition, Phys. Rev. Lett. **84**, 5180 (2000).
[7] S. Papanikolaou, R. M. Fernandes, E. Fradkin, P. W. Phillips, J. Schmalian, and R. Sknepnek, Universality of Liquid-Gas Mott Transitions at Finite Temperatures, Phys. Rev. Lett. **100**, 026408 (2008).
[8] P. Sémon and A.-M. S. Tremblay, Importance of subleading corrections for the Mott critical point, Phys. Rev. B **85**, 201101(R) (2012).
[9] M. Imada, A. Fujimori, and Y. Tokura, Metal-insulator transitions, Rev. Mod. Phys. **70**, 1039 (1998).
[10] V. Dobrosavljević, Introduction to metal-insulator transitions, in *Conductor-Insulator Quantum Phase Transitions* (Oxford University Press, Oxford, 2012), pp. 3–63.
[11] J. Vučičević, H. Terletska, D. Tanasković, and V. Dobrosavljević, Finite-temperature crossover and the quantum Widom line near the Mott transition, Phys. Rev. B **88**, 075143 (2013).
[12] H. Eisenlohr, S.-S. B. Lee, and M. Vojta, Mott quantum criticality in the one-band Hubbard model: Dynamical mean-field theory, power-law spectra, and scaling, Phys. Rev. B **100**, 155152 (2019).
[13] T. Li, S. Jiang, L. Li, Y. Zhang, K. Kang, J. Zhu, K. Watanabe, T. Taniguchi, D. Chowdhury, L. Fu *et al.*, Continuous Mott transition in semiconductor moiré superlattices, Nature (London) **597**, 350 (2021).
[14] J. E. Greedan, The rare earth-titanium (III) perovskite oxides—An isostructural series with a remarkable variation in physical properties, J. Less-Common Met. **111**, 335 (1985).
[15] S. M. Benjamin, N. F. Rieders, M. G. Smith, and J. J. Neumeier, From Ta_2S_5 wires to Ta_2O_5 and $Ta_2O_{5-x}S_x$, ACS Omega **6**, 5445 (2021).
[16] M.-K. Han, Y.-S. Jin, B. K. Yu, W. Choi, T.-S. You, and S.-J. Kim, Sulfur to oxygen substitution in BiOCuSe and its effect on the thermoelectric properties, J. Mater. Chem. A **4**, 13859 (2016).
[17] T. Katsufuji, Y. Taguchi, and Y. Tokura, Transport and magnetic properties of a Mott-Hubbard system whose bandwidth and band filling are both controllable: $R_{1-x}Ca_xTiO_{3+y/2}$, Phys. Rev. B **56**, 10145 (1997).
[18] M. C. O. Aguiar, V. Dobrosavljević, E. Abrahams, and G. Kotliar, Effects of disorder on the non-zero temperature Mott transition, Phys. Rev. B **71**, 205115 (2005).
[19] M. Y. Suárez-Villagrán, N. Mitsakos, T.-H. Lee, V. Dobrosavljević, J. H. Miller, and E. Miranda, Two-dimensional disordered Mott metal-insulator transition, Phys. Rev. B **101**, 235112 (2020).
[20] A. Goldman, Electrostatic gating of ultrathin films, Annu. Rev. Mater. Res. **44**, 45 (2014).
[21] S. Z. Bisri, S. Shimizu, M. Nakano, and Y. Iwasa, Endeavor of iontronics: From fundamentals to applications of ion-controlled electronics, Adv. Mater. **29**, 1607054 (2017).
[22] C. Leighton, Electrolyte-based ionic control of functional oxides, Nat. Mater. **18**, 13 (2019).
[23] H. Yuan, H. Shimotani, A. Tsukazaki, A. Ohtomo, M. Kawasaki, and Y. Iwasa, High-density carrier accumulation in ZnO field-effect transistors gated by electric double layers of ionic liquids, Adv. Funct. Mater. **19**, 1046 (2009).
[24] C. Leighton, T. Birol, and J. Walter, What controls electrostatic vs electrochemical response in electrolyte-gated materials? A perspective on critical materials factors, APL Mater. **10**, 040901 (2022).
[25] Y. Lee, C. Clement, J. Hellerstedt, J. Kinney, L. Kinnischtzke, X. Leng, S. D. Snyder, and A. M. Goldman, Phase Diagram of Electrostatically Doped $SrTiO_3$, Phys. Rev. Lett. **106**, 136809 (2011).
[26] K. Ueno, S. Nakamura, H. Shimotani, H. T. Yuan, N. Kimura, T. Nojima, H. Aoki, Y. Iwasa, and M. Kawasaki, Discovery of superconductivity in $KTaO_3$ by electrostatic carrier doping, Nat. Nanotechnol. **6**, 408 (2011).

[27] A. T. Bollinger, G. Dubuis, J. Yoon, D. Pavuna, J. Misewich, and I. Božović, Superconductor-insulator transition in $La_{2-x}Sr_xCuO_4$ at the pair quantum resistance, Nature (London) **472**, 458 (2011).

[28] X. Leng, J. Garcia-Barriocanal, B. Yang, Y. Lee, J. Kinney, and A. M. Goldman, Indications of an Electronic Phase Transition in Two-Dimensional Superconducting $YBa_2Cu_3O_{7-x}$, Phys. Rev. Lett. **108**, 067004 (2012).

[29] J. Garcia-Barriocanal, A. Kobrinskii, X. Leng, J. Kinney, B. Yang, S. Snyder, and A. M. Goldman, Electronically driven superconductor-insulator transition in electrostatically doped $La_2CuO_{4+\delta}$, Phys. Rev. B **87**, 024509 (2013).

[30] X. Leng, J. Pereiro, J. Strle, G. Dubuis, A. T. Bollinger, A. Gozar, J. Wu, N. Litombe, C. Panagopoulos, D. Pavuna, and I. Božović, Insulator to metal transition in WO_3 induced by electrolyte gating, npj Quantum Mater. **2**, 35 (2017).

[31] S. Bubel, A. J. Hauser, A. M. Glaudell, T. E. Mates, S. Stemmer, and M. L. Chabinyc, The electrochemical impact on electrostatic modulation of the metal-insulator transition in nickelates, Appl. Phys. Lett. **106**, 122102 (2015).

[32] R. Scherwitzl, P. Zubko, I. G. Lezama, S. Ono, A. F. Morpurgo, G. Catalan, and J. M. Triscone, Electric-field control of the metal-insulator transition in ultrathin $NdNiO_3$ films, Adv. Mater. **22**, 5517 (2010).

[33] E. Day-Roberts, T. Birol, and R. M. Fernandes, Contrasting ferromagnetism in pyrite FeS_2 induced by chemical doping versus electrostatic gating, Phys. Rev. Mater. **4**, 054405 (2020).

[34] J. Walter, B. Voigt, E. Day-Roberts, K. Heltemes, R. M. Fernandes, T. Birol, and C. Leighton, Voltage-induced ferromagnetism in a diamagnet, Sci. Adv. **6**, eabb7721 (2020).

[35] C. W. Stillwell, Crystal chemistry. IV. The structure of AX2, A2X3, AX3, AX4 compounds. Summary, J. Chem. Educ. **13**, 566 (1936).

[36] T. A. Bither, C. T. Prewitt, J. L. Gillson, P. E. Bierstedt, R. B. Flippen, and H. S. Young, New transition metal dichalcogenides formed at high pressure, Solid State Commun. **4**, 533 (1966).

[37] R. J. Bouchard, The preparation of pyrite solid solutions of the type $Fe_xCo_{1-x}S_2$, $Co_xNi_{1-x}S_2$, and $Cu_xNi_{1-x}S_2$, Mater. Res. Bull. **3**, 563 (1968).

[38] R. J. Bouchard, The preparation of single crystals of FeS_2, CoS_2, and NiS_2 pyrites by chlorine transport, J. Cryst. Growth **2**, 40 (1968).

[39] H. S. Jarrett, R. J. Bouchard, J. L. Gillson, G. A. Jones, S. M. Marcus, and J. F. Weiher, The metal-semiconductor phase diagram for $NiS_{2-x}Se_x$, Mater. Res. Bull. **8**, 877 (1973).

[40] S. Ogawa, S. Waki, and T. Teranishi, Magnetic and electrical properties of 3*d* transition metal disulfides having the pyrite structure, Int. J. Magn. **5**, 349 (1974).

[41] S. Brownridge, T. S. Cameron, H. Du, C. Knapp, R. Köppe, J. Passmore, J. M. Rautiainen, and H. Schnöckel, The highest bond order between heavier main-group elements in an isolated compound? Energetics and vibrational spectroscopy of $S_2I_4(MF_6)_2$ (M = As, Sb), Inorg. Chem. (Washington, DC, US) **44**, 1660 (2005).

[42] F. Gautier, G. Krill, M. F. Lapierre, and C. Robert, Influence of non-stoichiometry on the electrical and magnetic properties of NiS_2, Solid State Commun. **11**, 1201 (1972).

[43] R. Bouchard, J. Gillson, and H. Jarrett, The preparation and electrical properties of $NiSe_xS_{2-x}$ pyrites, Mater. Res. Bull. **8**, 489 (1973).

[44] T. A. Bither, R. J. Bouchard, W. H. Cloud, P. C. Donohue, and W. J. Siemons, Transition metal pyrite dichalcogenides. high-pressure synthesis and correlation of properties, Inorg. Chem. (Washington, DC, US) **7**, 2208 (1968).

[45] P. Wang, P. Somasundaram, J. Honig, and T. Pekarek, Single crystal growth and characterization of $NiSe_2$, Mater. Res. Bull. **32**, 1435 (1997).

[46] S. Yano, D. Louca, J. Yang, U. Chatterjee, D. E. Bugaris, D. Y. Chung, L. Peng, M. Grayson, and M. G. Kanatzidis, Magnetic structure of $NiS_{2-x}Se_x$, Phys. Rev. B **93**, 024409 (2016).

[47] W. Folkerts, G. A. Sawatzky, C. Haas, R. A. de Groot, and F. U. Hillebrecht, Electronic structure of some 3*d* transition-metal pyrites, J. Phys. C: Solid State Phys. **20**, 4135 (1987).

[48] A. Fujimori, K. Mamiya, T. Mizokawa, T. Miyadai, T. Sekiguchi, H. Takahashi, N. Mori, and S. Suga, Resonant photoemission study of pyrite-type NiS_2, CoS_2 and FeS_2, Phys. Rev. B **54**, 16329 (1996).

[49] K. Iwaya, Y. Kohsaka, S. Satow, T. Hanaguri, S. Miyasaka, and H. Takagi, Evolution of local electronic states from a metal to a correlated insulator in a $NiS_{2-x}Se_x$ solid solution, Phys. Rev. B **70**, 161103(R) (2004).

[50] X. Yao, J. M. Honig, T. Hogan, C. Kannewurf, and J. Spalek, Electrical properties of $NiS_{2-x}Se_x$, Phys. Rev. B **54**, 17469 (1996).

[51] J. Kuneš, L. Baldassarre, B. Schächner, K. Rabia, C. A. Kuntscher, D. M. Korotin, V. I. Anisimov, J. A. McLeod, E. Z. Kurmaev, and A. Moewes, Metal-insulator transition in $NiS_{2-x}Se_x$, Phys. Rev. B **81**, 035122 (2010).

[52] G. Han, S. Choi, H. Cho, B. Sohn, J.-G. Park, and C. Kim, Structural investigation of the insulator-metal transition in $NiS_{2-x}Se_x$ compounds, Phys. Rev. B **98**, 125114 (2018).

[53] C.-Y. Moon, H. Kang, B. G. Jang, and J. H. Shim, Composition and temperature dependent electronic structures of $NiS_{2-x}Se_x$ alloys: First-principles dynamical mean-field theory, Phys. Rev. B **92**, 235130 (2015).

[54] J. A. Wilson, The Mott transition for binary compounds, including a case study of the pyrite system $Ni(S_{1-x}Se_x)_2$, in *Metallic and Non-metallic States of Matter*, edited by P. P. Edwards and C. N. R. Rao (Taylor and Francis Ltd., London, 1985), pp. 215–260 .

[55] A. Y. Matsuura, H. Watanabe, C. Kim, S. Doniach, Z.-X. Shen, T. Thio, and J. W. Bennett, Metal-insulator transition in $NiS_{2-x}Se_x$ and the local impurity self-consistent approximation model, Phys. Rev. B **58**, 3690 (1998).

[56] B. G. Jang, G. Han, I. Park, D. Kim, Y. Y. Koh, Y. Kim, W. Kyung, H.-D. Kim, C.-M. Cheng, K.-D. Tsuei, K. D. Lee, N. Hur, J. H. Shim, C. Kim, and G. Kotliar, Direct observation of kink evolution due to Hund's coupling on approach to metal-insulator transition in $NiS_{2-x}Se_x$, Nat. Commun. **12**, 1208 (2021).

[57] G. Kotliar, S. Y. Savrasov, K. Haule, V. S. Oudovenko, O. Parcollet, and C. A. Marianetti, Electronic structure calculations with dynamical mean-field theory, Rev. Mod. Phys. **78**, 865 (2006).

[58] K. Haule, C.-H. H. Yee, and K. Kim, Dynamical mean-field theory within the full-potential methods: Electronic structure of $CeIrIn_5$, $CeCoIn_5$, and $CeRhIn_5$, Phys. Rev. B **81**, 195107 (2010).

[59] A. Paul and T. Birol, Applications of DFT + DMFT in materials science, Annu. Rev. Mater. Res. **49**, 31 (2019).

[60] S. Hameed, B. Voigt, J. Dewey, W. Moore, D. Pelc, B. Das, S. El-Khatib, J. Garcia-Barriocanal, B. Luo, N. Seaton, G. Yu, C. Leighton, and M. Greven, Electrochemically-driven insulator-metal transition in ionic-liquid-gated antiferromagnetic Mott-insulating NiS_2 single crystals, arXiv:2201.00340.

[61] K. Haule, Structural predictions for correlated electron materials using the functional dynamical mean field theory approach, J. Phys. Soc. Jpn. **87**, 041005 (2018).

[62] P. Blaha, K. Schwarz, F. Tran, R. Laskowski, G. K. Madsen, and L. D. Marks, WIEN2k: An APW+lo program for calculating the properties of solids, J. Chem. Phys. **152**, 074101 (2020).

[63] H. Shinaoka, J. Otsuki, M. Ohzeki, and K. Yoshimi, Compressing Green's function using intermediate representation between imaginary-time and real-frequency domains, Phys. Rev. B **96**, 035147 (2017).

[64] K. Haule, T. Birol, and G. Kotliar, Covalency in transition-metal oxides within all-electron dynamical mean-field theory, Phys. Rev. B **90**, 075136 (2014).

[65] S. Mandal, K. Haule, K. M. Rabe, and D. Vanderbilt, Systematic beyond-DFT study of binary transition metal oxides, npj Comput. Mater. **5**, 115 (2019).

[66] K. Haule, Exact Double Counting in Combining the Dynamical Mean Field Theory and the Density Functional Theory, Phys. Rev. Lett. **115**, 196403 (2015).

[67] E. Nowack, D. Schwarzenbach, and T. Hahn, Charge densities in CoS_2 and NiS_2 (pyrite structure), Acta Crystallogr., Sect. B: Struct. Sci. **47**, 650 (1991).

[68] S. Li and T. Birol, Free-Carrier-Induced Ferroelectricity in Layered Perovskites, Phys. Rev. Lett. **127**, 087601 (2021).

[69] P. Blaha, K. Schwarz, G. K. Madsen, D. Kvasnicka, J. Luitz *et al.*, Wien2k user's manual, An augmented plane wave + local orbitals program for calculating crystal properties (2001), http://wien2k.at/.

[70] S. Ogawa, Specific heat study of magnetic ordering and band structure of 3*d* transition metal disulfides having the pyrite structure, J. Phys. Soc. Jpn. **41**, 462 (1976).

[71] J. B. Goodenough, Conceptual phase diagram and its application to the spontaneous magnetism of several pyrites, J. Solid State Chem. **3**, 26 (1971).

[72] G. L. Zhao, J. Callaway, and M. Hayashibara, Electronic structures of iron and cobalt pyrites, Phys. Rev. B **48**, 15781 (1993).

[73] J. M. Hastings and L. M. Corliss, Ordered moment of NiS_2, IBM J. Res. Dev. **14**, 227 (1970).

[74] T. Higo and S. Nakatsuji, Magnetization anomaly due to the non-coplanar spin structure in NiS_2, J. Phys. Soc. Jpn. **84**, 053702 (2015).

[75] J. A. Wilson and G. D. Pitt, Metal-insulator transition in NiS_2, Philos. Mag. (1798–1977) **23**, 1297 (1971).

[76] S. Friedemann, H. Chang, M. B. Gamża, P. Reiss, X. Chen, P. Alireza, W. A. Coniglio, D. Graf, S. Tozer, and F. M. Grosche, Large Fermi surface of heavy electrons at the border of mott insulating state in NiS_2, Sci. Rep. **6**, 25335 (2016).

[77] See Supplemental Material at http://link.aps.org/supplemental/10.1103/PhysRevB.107.085150 for the results of alternate analytic continuation calculations and polynomial fits to determine quasiparticle weight.

[78] H. T. Dang, J. Mravlje, A. Georges, and A. J. Millis, Electronic correlations, magnetism, and Hund's rule coupling in the ruthenium perovskites $SrRuO_3$ and $CaRuO_3$, Phys. Rev. B **91**, 195149 (2015).

[79] R. Bulla, T. A. Costi, and D. Vollhardt, Finite-temperature numerical renormalization group study of the Mott transition, Phys. Rev. B **64**, 045103 (2001).

[80] M. Capone, G. Sangiovanni, C. Castellani, C. Di Castro, and M. Grilli, Phase Separation Close to the Density-Driven Mott Transition in the Hubbard-Holstein Model, Phys. Rev. Lett. **92**, 106401 (2004).

[81] M. M. Radonjić, D. Tanasković, V. Dobrosavljević, K. Haule, and G. Kotliar, Wigner-Mott scaling of transport near the two-dimensional metal-insulator transition, Phys. Rev. B **85**, 085133 (2012).